IEEE Access
Multidisciplinary ⋮ Rapid Review ⋮ Open Access Journal

Received October 22, 2020, accepted November 3, 2020, date of publication November 16, 2020,
date of current version November 25, 2020.

Digital Object Identifier 10.1109/ACCESS.2020.3038252

Dynamics Modeling Analysis and Experiment of the Guidance Control System of High-Speed Maglev Train

BOWEN LI[1], CHUNXIA ZHAO[2], XIAOLONG LI[1], AND ZHIQIANG LONG[1]
[1]College of Intelligence Science and Technology, National University of Defense Technology, Changsha 410073, China
[2]PLA 63850 Unit, Baicheng 137001, China

Corresponding author: Zhiqiang Long (lzq@maglev.cn)

This work was supported by the National Key Technology Research and Development Program of China under Grant 2016YFB1200602.

ABSTRACT The guidance control system of the high-speed maglev enable that the maglev can travel along the center line of track. When the maglev passes through curve, the guidance control system also provides guidance force. When the maglev operates on the track, the friction between guidance electromagnet and track happens sometimes. This problem will pose a great threat to the safety of maglev running. However, other studies have failed to reflect the actual operation very well. In order to give a reasonable explanation for problems happened in actual test, the dynamics model of the guidance control system in high-speed maglev is established in this paper. The curve operation simulation was carried out, and the reason of the friction problem was analyzed through the results of simulation. Finally, an actual running test was carried out. The result of test shows that the high-speed maglev guidance control model established in this paper is effective. This model can provide an platform for analyzing the motion of guidance control units of the high-speed maglev train, further provide a model reference for the design and optimization of the control algorithm.

INDEX TERMS Dynamics modeling, high-speed maglev, guidance control system, motion analysis.

I. INTRODUCTION

Compared with the high-speed wheel-rail transportation system, the high-speed maglev has the advantages of smaller turning radius, lower energy consumption, lower mechanical wear, more safety and easy maintenance [1]–[5]. At present, China is developing a new generation of high-speed maglev train with a speed of 600 km/h. In the future, high-speed maglev trains have broad application prospects all over the world.

The overall structure of the guidance system of high-speed maglev is shown in Fig.1. The guidance control system is mainly composed of guidance controller, guidance electromagnet, suspension device, bogie and carriage. The goal of guidance control is to enable high-speed maglev trains to run in the center of the track.

The research on the guidance system of high-speed maglev train mainly includes two aspects: guidance control research and guidance dynamics research. The research on guidance control mainly focuses on the research of control algorithm. Aiming at the problems of large variation of working current and track irregularity, Hao *et al.* designed robust controller and adaptive controller [6]–[9]; Chang *et al.* designed yaw controller for the train yaw control [10]; Min *et al.* analyzed the active guidance control system of medium speed maglev train [11]. Lee *et al.* proposed a new electrical guidance device, designed a new cascade sliding mode controller and a cascade sliding mode based genetic algorithm control [12].

There are mainly two approaches to the study of guidance dynamics. The first way is to establish the dynamics equation of rigid body by force analysis. Zhao *et al.* analyzed the working state of the guidance system when the single bogie system was running in the curve [13]. Wu *et al.* established the guidance dynamics model of a single train on straight track, but did not consider the system model under the condition of curve [14]. The second research way is to build a virtual prototype of vehicle by using dynamics simulation software. Ye *et al.* carried out dynamics modeling and simulation of the vehicle with SIMPACK software, and

The associate editor coordinating the review of this manuscript and approving it for publication was Hassen Ouakad.

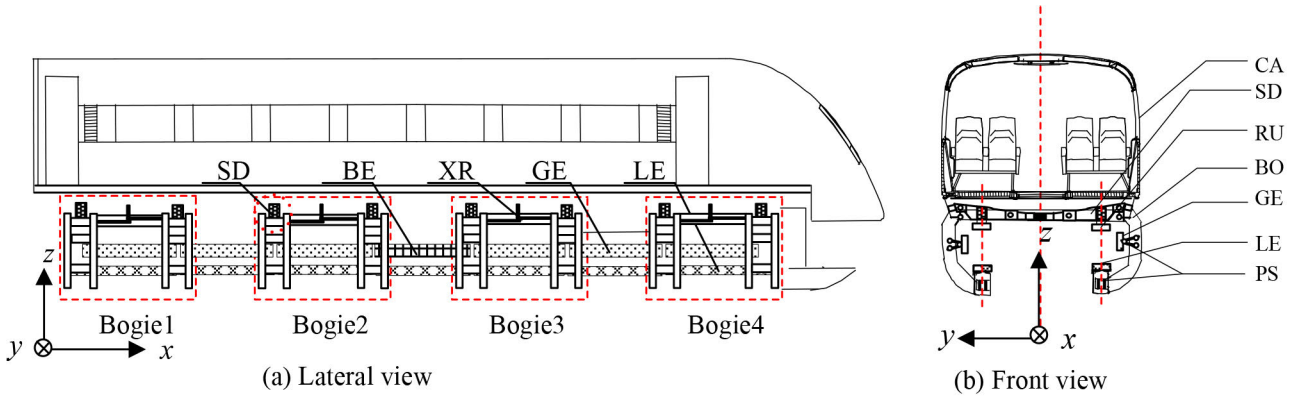

FIGURE 1. Total structure of high-speed maglev train. CA:Carriage. SD:Suspension device. RU:Runner. BO:Bogie. GE:Guidance electromagnet. LE:Levitation electromagnet. PS:Primary suspension device. BE:Eddy-current-brake electromagnet. XR:x-direction rod.

obtained the vertical and transverse dynamics response characteristics of some rigid bodies of the vehicle system along the track [15]–[17]. Piao *et al.* built the dynamics model of vehicle system through the collaborative simulation platform, further the lateral dynamics response of parts of rigid bodies when the system passed through the curve, and the role of the pendulum rod in the secondary suspension device are analyzed [18]–[22].

However, other studies have failed to reflect the actual operation very well. First of all, too much simplification are made in the model of guidance control system in previous research about the guidance control algorithm. Model after simplifying can neither reflect the guidance dynamics characteristics nor guide the work of parameter adjustment effectively. Consequently, it is always time-consuming and difficult to adjust the controller parameters in the test, which brings a lot of inconvenience to the debugging work. Secondly, most of the research in guidance dynamics field is aimed at analyzing the lateral vibration response of vehicle and the dynamics characteristics of rigid bodies. However, they have failed to give the working state of guidance control units. Last but not least, when the maglev operates on the track, the friction between guidance electromagnet and track happens sometimes. This problem will pose a great threat to the safety of maglev running. However, the reasonable explanation for this problem has rarely been examined directly.

In order to give a reasonable explanation for problems happened in actual test and accurately get the working state of the guidance control system, a dynamics model of the guidance control system is established in this paper. At first, the structure of the high-speed maglev train is analyzed; The parameter model of various components are established in section II. Secondly, the lateral motion equations of the rigid bodies are established; The interaction models of the primary suspension device and the secondary suspension device are derived in section III. Thirdly, the control strategy of guidance system is proposed in section IV. Fourthly, a simulation model of the guidance control system of the whole maglev is established in section V; The operation situation of the guidance control system through a curve line is simulated; The working state of the guidance system is analyzed. Finally, the vehicle operation test was carried out on the test line in Jiading, Shanghai; The accuracy of the simulation model was verified with the test results in section VI.

II. MAGLEV STRUCTURE AND PARAMETRIC MODEL

A. THE OVERALL STRUCTURE AND ASSEMBLY PRINCIPLE OF THE VEHICLE

The overall structure of the high-speed maglev train is shown in Fig.1. It is mainly composed of carriage, secondary suspension devices, bogies, primary suspension devices and electromagnets. Carriage and bogies are connected by secondary suspension devices; Electromagnets and bogies are connected by primary suspension devices. There are three types of electromagnets, including suspension electromagnet, guidance electromagnet and eddy-current-braking electromagnet.

The suspension system and the guidance system are basically decoupled through the suspension device. Therefore, in order to simplify the research, the influence of the movement in the direction of suspension will be ignored. In addition, suspension electromagnet and eddy-current-braking electromagnet are ignored when building the guidance dynamics.

The following step is to determine the parametric models of the functional components and connecting components of the guidance system. Functional components of guidance system mainly include the guidance electromagnet, bogie and carriage. Connecting components of guidance system mainly include the primary suspension device and the secondary suspension device.

B. BOGIE STRUCTURE

The real structure of a single bogie is shown in Fig.2, which is mainly composed of four suspension frames of which shape like "C" type, two cross beams and one longitudinal beam. Each "C" type suspension frame contains a pair of support arms. There are connecting pieces between the support arms. Each cross beam is formed by two beams, bolster support and air spring support.

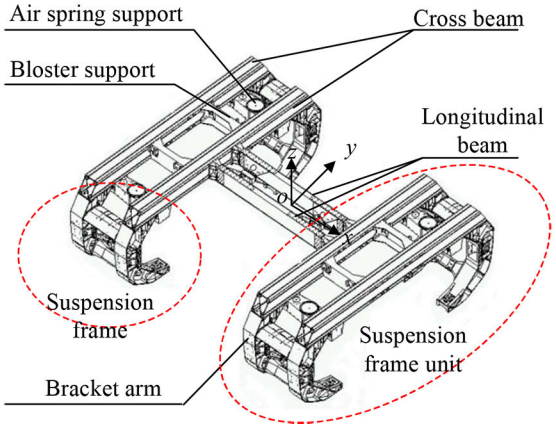

FIGURE 2. Structure of single bogie system of maglev.

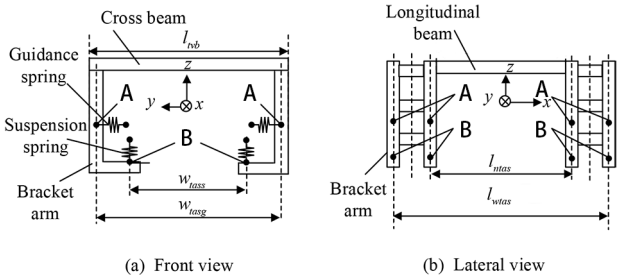

FIGURE 3. Parametric model of single bogie system.

In the research of guidance dynamics, if the bogie is completely considered as an elastic body, its mathematical modeling is relatively complicated, and it is difficult to obtain an analytical model of the bogie. Therefore, in order to simplify the research, the elastic bogie is equivalent to the rigid bogie and its attached guidance arm springs. The parameterization model is shown in Fig.3. The points masked "A" and "B" are the connection point of suspension spring on the bogie. w_{tass} and w_{tasg} are the distances in y-direction between the connection points of bogie. l_{ntas} and l_{wtas} are the distances in x-direction between the connection points of bogie.

C. PRIMARY SUSPENSION DEVICE STRUCTURE

The guidance primary suspension device is composed of a triangle hinge and an anti-roll rod. The connection method is shown in Fig.4.

Triangle hinge includes one triangle bracket, two rubber ball joints. The triangle bracket is a rigid bracket, whose two ends are connected by two rubber ball joints.

One end of the anti-roll rod is connected with the bogie through the rubber ball joint, and the other end is connected with the support of guidance electromagnet through a metal pin.

Since the two anti-roll rods at the front and back ends of the guidance electromagnet are installed in the diagonal direction of the electromagnet, the electromagnet can be restricted from rolling relative to the bogie. Therefore, the guidance suspension device can provide 5 degree-of-freedom relative motions for the guidance electromagnet and the bogie.

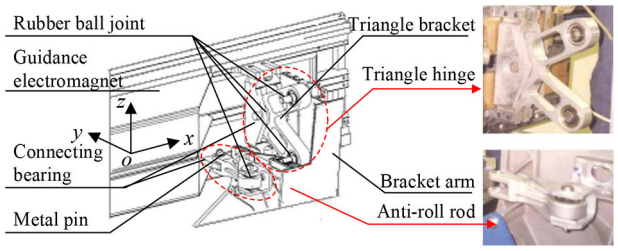

FIGURE 4. Structure of guidance primary suspension device.

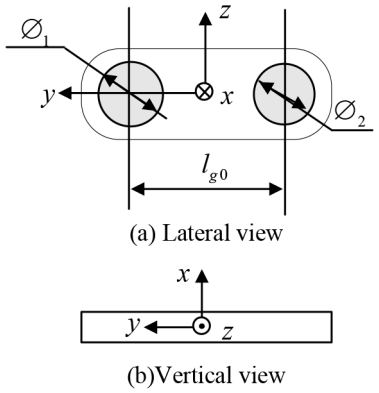

FIGURE 5. Parametric model of guidance primary suspension device.

Relative motion compensation is achieved through the deformation of each ball joint hinge in the device. As is shown in Fig.5, the equivalent parametric model is a connecting rod device with a rigid rod in the middle and two rubber ball joints at both ends. The mass of the rigid rod itself can be ignored. l_{g0} represents the distance between two rubber balls.

D. SECONDARY SUSPENSION DEVICE STRUCTURE

The structure of the secondary suspension device is shown in Fig.6. It is mainly composed of anti-roll metal rubber parts, rubber ball joints, bolsters, air springs, pendulum rods, z-direction supports, y-direction auxiliary springs/limit springs and other components. The assembly principle is as follows:

The end of the bolster is connected with the anti-roll metal rubber part, passing through the bolster frame on the bogie beam. The bolster and the frame are connected by rubber ball joints, which can rotate longitudinally around the frame.

The bottom of the air spring is installed on the air spring support on the bogie beam, and the top of it is nested in the groove of the bolster arm. The air spring and the beam only transfer to the z-direction load, not to the y-direction load.

The ends of the bolster and the pendulum rod are connected by smooth metal ball joints, which can swing freely between each other. So are the pendulum rod and the z-direction support. The z-direction support and the carriage floor are rigidly connected.

In order to distribute the load uniformly along the longitudinal direction of the train, the effective bearing area of the air spring on the suspension frame at the end of the train is half of the middle air spring. In condition that the pressure of

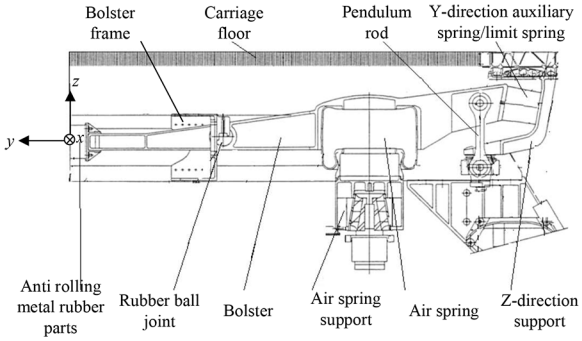

FIGURE 6. Structure of second suspension device.

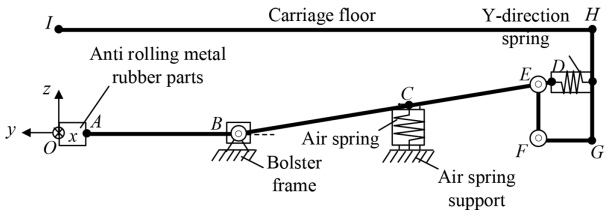

FIGURE 7. Parametric model of guidance primary suspension device.

all air spring is the same, the supporting force of the end air spring is half of other air springs.

In order to distribute the load uniformly along the longitudinal direction of the train, as shown in Fig.1, on the suspension frames 2, 3, 6 and 7, y-direction auxiliary springs are installed between the bolsters and the z-direction support. On the suspension frame 1, 4, 5 and 8, y-direction limit spring is installed between the bolster and the z-direction support, which only works when the displacement exceeds 90 mm.

According to its assembly principle, it is equivalent to the model shown in the Fig.7. The total lateral stiffness of the secondary suspension device only depends on the swing stiffness of the pendulum rod EF and the lateral stiffness of the y-direction spring. In addition, since the height change of the carriage caused by the deformation of the secondary suspension device is much smaller than the height of the carriage, when analyzing the lateral stiffness, the vertical height change caused by the dynamics adjustment of the secondary suspension device is ignored. Approximately, the height of the center of mass of the carriage from the track surface remains constant.

E. LINE PARAMETER MODEL

In order to simulate the operation of the maglev train, it is necessary to model the running line. Line that used in simulation is shown in Fig.8. This simulation line is designed based on a curve at Jiading test line in Shanghai. In Fig.8, L1 and L2 represent straight line segments, T1 and T2 represent transition curve segments, C represents circular curve segments. The starting point of the track center line is selected as the origin o^0 of the inertial coordinate system. R is the radius of curvature of the circular curve, ρ is the curvature of the whole line, θ_m is the maximum cross slope angle of the track.

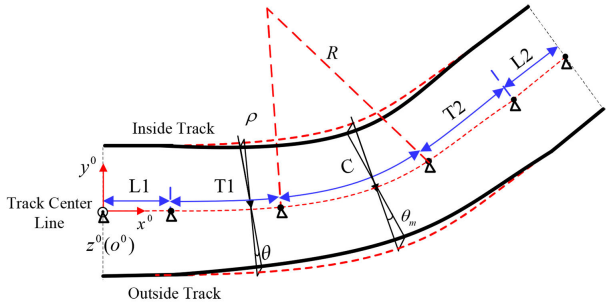

FIGURE 8. Simulation model of line on which the maglev train model operates.

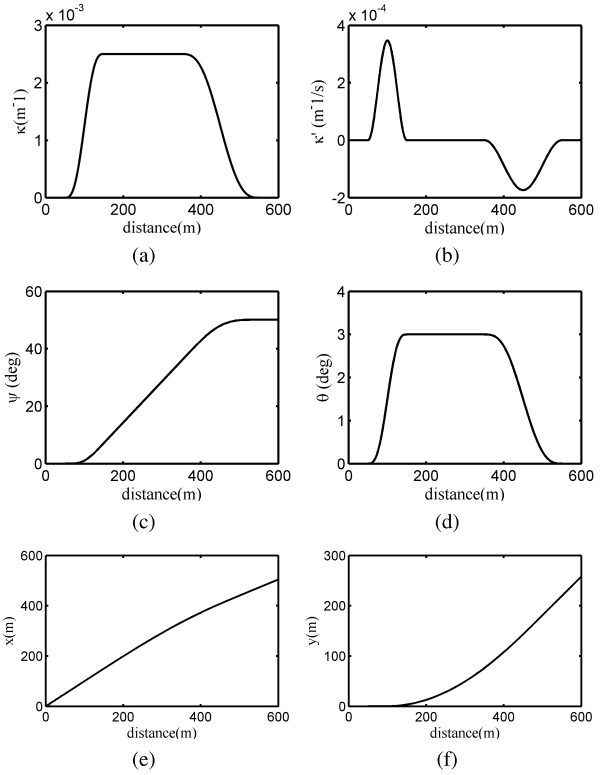

FIGURE 9. Parameters of simulation line. (a) Curvature of the line κ. (b) The first order derivative of curvature κ'. (c) Direction angle ψ. (d) Cross slope angle θ. (e) X-coordinate x. (f) Y-coordinate y.

The curve of various parameters of the line following distance is shown in Fig.9.

III. SYSTEM DYNAMICS MODEL

A. DYNAMICS MODELING PROCESS

When the train runs at a constant speed without the external interference of the vehicle system and the relative movement between the rigid bodies and the track, the traction movement of each rigid body along the track's longitudinal direction can be regarded as moving together following the track coordinate system $o^{rn}x^{rn}y^{rn}z^{rn}(n = 1 \sim 7)$shown in Fig.10. In this figure, the origin of the coordinate system $o^{rn}(n = 1, 2, \ldots 7)$ moves along the track centerline at a speed V. The arc length of the track centerline between the origins of two adjacent coordinate systems is always equals $l_t = 3.096m$.

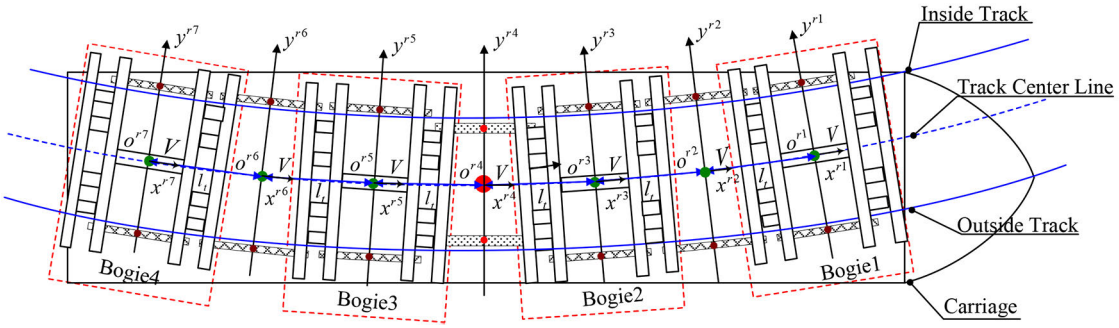

FIGURE 10. Track coordinate system of maglev during the process of passing curve.

The x^{rn}-axis is along the tangent direction of the track centerline. The y^{rn}-axis is along the track The direction of the normal to the center line within the track plane. The z^{rn}-axis is perpendicular to the track surface.

When modeling the guidance dynamics, the track coordinate system in Fig.10 is selected as the implicated coordinate system. The movement of the rigid bodies of the guidance system in the inertial coordinate system is decomposed into the translational movement following the track coordinate system and the rotational motion of the rigid body around the axis that is perpendicular to the track surface. Consequently, the guidance dynamics modeling of each rigid body can be classified into the same question. As long as the dynamics model of a single rigid body is involved in the track operation, the dynamics model of the overall guidance system can be obtained.

If the traction running speed V and running time t of the train are known, it is easy to get the position and posture of the coordinate system $o^{rn}x^{rn}y^{rn}z^{rn}$ in the inertial system, so as to determine the longitudinal traction operation law of each rigid body in the guidance system.

B. RIGID BODY COORDINATE SYSTEM ESTABLISHMENT

As shown in Fig.11, the motion of a single rigid body involved in the track can be described by three sets of coordinate systems, including the inertial coordinate system $o^0x^0y^0z^0$, the track involved coordinate system, namely the track coordinate system $o^rx^ry^rz^r$ and the rigid body connected coordinate system, namely the rigid body coordinate system $o^bx^by^bz^b$.

The inertial coordinate system is a fixed coordinate system, which is connected to the ground and is used to describe the track line. The origin o^0 is selected at the starting point of the track centerline, and the x^0-axis is along the tangent direction of the center line.

The track coordinate system is a dynamics coordinate system. the origin o^r moves along the track centerline at a speed V. The x^r-axis is along the tangent direction of the track centerline. The y^r-axis points to the inside of the curve within the track surface.

The rigid body coordinate system is a conjoined coordinate system. The origin o^b is at the mass center of the rigid body. The three coordinate axes are the inertia principal axes of the rigid body in turn. Since the guidance dynamics modeling only considers the deviation component of the rigid body center of mass along the lateral direction of the track, so the projection of point o^b on the track surface will be on y^r-axis.

In order to describe the process of rotation transformation from the inertial coordinate system to the track coordinate system vividly, the track centerline coordinate system $o^{rc}x^{rc}y^{rc}z^{rc}$ is added in the figure, where the plane $x^{rc}-y^{rc}$ and the plane of the inertial coordinate system x^0-y^0 are coplanar.

It is known that the translation and rotation transformation relationships between the inertial coordinate system, the track centerline coordinate system, the track coordinate system and the rigid body coordinate system in Fig.9 are as follows

$$\begin{aligned} o^0x^0y^0z^0 &\xrightarrow[P(r_r)]{A_3(\psi)} o^{rc}x^{rc}y^{rc}z^{rc} \xrightarrow[A_1(-\theta)]{} o^rx^ry^rz^r \\ o^rx^ry^rz^r &\xrightarrow[P(r)]{A_3(\phi)} o^bx^by^bz^b \end{aligned} \tag{1}$$

Among them: P represents the translation transformation matrix; A represents the rotation transformation matrix, and its subscripts "1" and "3" respectively represent counterclockwise rotation around the x-axis and z-axis of the coordinate system; r_r is the translation vector from the inertial coordinate system to the track centerline coordinate system. r is the translation vector from the track coordinate system to the rigid body coordinate system. r_c is the translation vector from the inertial coordinate system to the rigid body coordinate system. ψ is the direction angle of the track centerline. θ is the cross slope angle of the line. φ is the yaw angle of the rigid body relative to the track.

In the relational formula, the specific expression of the rotation transformation matrix between each coordinate system is as follows:

The rotation transformation matrix from the inertial coordinate system to the track coordinate system is

$$\boldsymbol{A}_0^r = \boldsymbol{A_1}(-\theta)\boldsymbol{A_3}(-\psi) \tag{2}$$

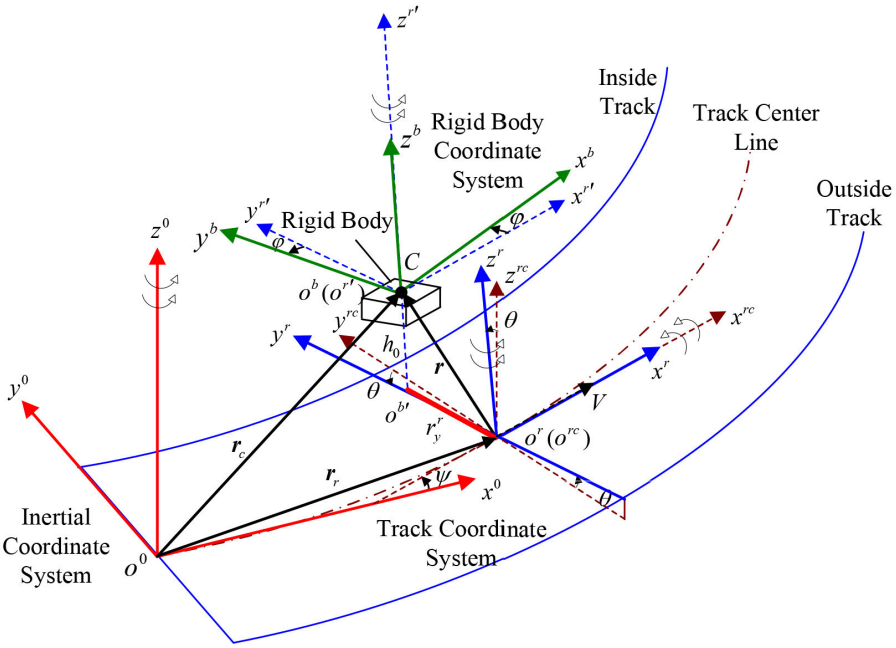

FIGURE 11. Three Coordinate systems used for the description of the motion of single rigid body.

The rotation transformation matrix from the track coordinate system to the inertial coordinate system is

$$\boldsymbol{A}_r^0 = (\boldsymbol{A}_{\boldsymbol{0}}^{\boldsymbol{r}})^{-1} \tag{3}$$

The rotation transformation matrix from the track coordinate system to the rigid body coordinate system is

$$\boldsymbol{A}_r^b = \boldsymbol{A}_{\boldsymbol{3}}(\varphi) \tag{4}$$

The rotation transformation matrix from the rigid body coordinate system to the track coordinate system is:

$$\boldsymbol{A}_b^r = (\boldsymbol{A}_{\boldsymbol{3}}(\varphi))^{-1} \tag{5}$$

The rotation transformation matrix from the inertial coordinate system to the rigid body coordinate system is

$$\boldsymbol{A}_0^b = \boldsymbol{A}_{\boldsymbol{3}}(\varphi)\boldsymbol{A}_{\boldsymbol{1}}(\theta)\boldsymbol{A}_{\boldsymbol{3}}(\psi) \tag{6}$$

The rotation transformation matrix from the rigid body coordinate system to the inertial coordinate system is

$$\boldsymbol{A}_b^0 = (\boldsymbol{A}_{\boldsymbol{0}}^{\boldsymbol{b}})^{-1} \tag{7}$$

It is known that vectors are often located in different coordinate systems, so it is impossible to deal with them without unifying. As a result, the vectors in different coordinate systems must be converted to the same coordinate system for calculation by using (2) to (7).

C. TRANSLATIONAL AND ROTATIONAL MOTION EQUATIONS OF RIGID BODY

The guidance electromagnets, bogies and carriages in the guidance system can all be regarded as rigid bodies. The movement of the rigid body along the y-axis of the track coordinate system under the action of external force is called lateral movement, and the movement along the x-axis is called longitudinal movement. In the dynamics research of the guidance system, the lateral dynamics performance of the vehicle is the core of the research, so the lateral motion of the rigid body is more worthy of attention. Specifically, the lateral motion of a rigid body can be divided into translational motion along the y^r-axis of the track coordinate system and rotational motion around the z^r-axis. The content of this section is mainly to establish the lateral deviation equation and lateral yaw equation of a rigid body through the theorem of the center of mass motion of the rigid body and the theorem of moment of momentum.

1) TRANSLATIONAL MOTION EQUATIONS

From the center of mass motion theorem, the motion equation of the center of mass of a rigid body is

$$m\boldsymbol{a}_c = \boldsymbol{F}_c^e \tag{8}$$

Among them, m is the mass of the rigid body, $\boldsymbol{a}_c$ is the acceleration of the rigid body's center of mass in the inertial system, and $\boldsymbol{F}_c^e$ is the resultant external force received by the rigid body.

According to the acceleration composition theorem, the acceleration in the track coordinate system can be expressed as

$$\boldsymbol{a}_c = \boldsymbol{a}_e + \boldsymbol{a}_k + \boldsymbol{a}_r \tag{9}$$

where $\boldsymbol{a}_e$ represents the implicated acceleration of the rigid body in the track coordinate system, $\boldsymbol{a}_k$ represents the coriolis acceleration, and $\boldsymbol{a}_r$ represents the relative acceleration. The following equation can be obtained by combining (8) and (9).

$$m\boldsymbol{a}_r = \boldsymbol{F}_c^e - m\boldsymbol{a}_e - m\boldsymbol{a}_k^r \tag{10}$$

Converting (10) to the track coordinate system

$$m\ddot{\boldsymbol{r}}^r = \boldsymbol{F}_c^r + \boldsymbol{F}_e^r + \boldsymbol{F}_k^r \tag{11}$$

The implicated inertial force of the rigid body in the track coordinate system is

$$\boldsymbol{F}_e^r = m\boldsymbol{a}_e^r = m[\boldsymbol{\omega}_e^r \times \boldsymbol{V}_o^r + \boldsymbol{\varepsilon}_e^r \times \boldsymbol{r}^r + \boldsymbol{\omega}_e^r \times (\boldsymbol{\omega}_e^r \times \boldsymbol{r}^r)] \tag{12}$$

The coriolis force received by the rigid body is

$$\boldsymbol{F}_k^r = m\boldsymbol{a}_k^r = 2\boldsymbol{\omega}_e^r \times \dot{\boldsymbol{r}}^r \tag{13}$$

where, the superscript r represents the vector of each physical quantity in the track coordinate system.

The rotational angular velocity of the track coordinate system in the inertial system is $\boldsymbol{\omega}_e$. According to Euler's theorem of rotation, the projection of $\boldsymbol{\omega}_e$ in the track coordinate system is $\boldsymbol{\omega}_e^r$, whose expression is

$$\begin{aligned}\boldsymbol{\omega}_e^r &= \begin{bmatrix}\omega_{ex}^r \\ \omega_{ey}^r \\ \omega_{ez}^r\end{bmatrix} = \mathbf{A}_e^r \begin{bmatrix}\dot{\psi} \\ -\dot{\theta} \\ -\dot{\varphi}\end{bmatrix}\Bigg|_{\varphi=0} \\ &= \begin{bmatrix}-\dot{\theta} \\ -\dot{\psi}sin\theta \\ \dot{\psi}cos\theta\end{bmatrix}\end{aligned} \tag{14}$$

$$\mathbf{A}_e^r = \begin{bmatrix}-sin\theta sin\varphi & cos\varphi & 0 \\ -sin\theta sin\varphi & -sin\varphi & 0 \\ cos\theta & 0 & 1\end{bmatrix} \tag{15}$$

Among them, $\mathbf{A}_e^r$ represents the rotation change matrix from the inertial system to the track coordinate system. ω_{ex}^r, ω_{ey}^r and ω_{ez}^r represent the components of the track coordinate system's rotational angular velocity along the x, y, and z axes of the projection of the track coordinate system respectively.

Derivation of the (15), namely the angular acceleration of the track coordinate system rotation can be obtained as

$$\boldsymbol{\varepsilon}_e^r = \dot{\boldsymbol{\omega}}_e^r = \begin{bmatrix}\dot{\omega}_{ex}^r \\ \dot{\omega}_{ey}^r \\ \dot{\omega}_{ez}^r\end{bmatrix} = \begin{bmatrix}-\ddot{\theta} \\ -\ddot{\psi}sin\theta - \dot{\psi}\dot{\theta}cos\theta \\ \ddot{\psi}cos\theta - \dot{\psi}\dot{\theta}sin\theta\end{bmatrix} \tag{16}$$

The projection of the velocity vector $\boldsymbol{V}_o^r$ in the track coordinate system is

$$\boldsymbol{V}_o^r = \begin{bmatrix}V & 0 & 0\end{bmatrix} \tag{17}$$

In the coordinate system shown in Fig.11, it can be seen that $\boldsymbol{r}^r = \begin{bmatrix}0 & r_y^r & h\end{bmatrix}$, $\dot{\boldsymbol{r}}^r = \begin{bmatrix}0 & \dot{r}_y^r & h\end{bmatrix}$,where h represents the distance from the center of mass of the rigid body to the track coordinate system, r_y^r represents the distance along y-axis from the track coordinate system to the rigid body coordinate system.

Substitute (14) to (17) into (12) and (13), the components of traction inertia force and coriolis force along the y^r-axis of the track coordinate system can be obtained

$$F_{ey}^r \approx -mV^2\kappa cos\theta, F_{ky}^r = 0 \tag{18}$$

where V represents the speed of the track coordinate system along the x^r-axis, namely the running speed of the vehicle. κ represents the curvature of the horizontal curve of the track. θ represents the cross slope angle of the track.

Substituting (18) into (11), the deviation motion equation of the rigid body along the y^r-axis can be obtained

$$m\ddot{r}_y^r = F_{cy}^r + F_{ey}^r + F_{ky}^r = F_{cy}^r + F_{ey}^r \tag{19}$$

2) ROTATIONAL MOTION EQUATIONS

From the theorem of the moment of momentum of the mass point system relative to the center of mass, it can be seen that the derivative of the moment of momentum $\boldsymbol{L}_c$ of the rigid body to the center of mass with respect to time is equal to the principal torque of the external force system to the rigid body $\boldsymbol{M}_c^b$

$$\frac{d\boldsymbol{L}_c}{dt} = \boldsymbol{M}_c^b \tag{20}$$

The rigid body coordinate system is used as the calculation coordinate system to derive the fixed-axis rotation equation. The origin o^b of the rigid body coordinate system is on the rigid body's center of mass. Each coordinate axis is located on the rigid body's inertial principal axis. Therefore, the inertia tensor matrix of the rigid body relative to the center of mass can be expressed as

$$\boldsymbol{I} = \begin{bmatrix}I_x & 0 & 0 \\ 0 & I_y & 0 \\ 0 & 0 & I_z\end{bmatrix} \tag{21}$$

Among them, I_x, I_y and I_z are the torques of inertia of the module about the x^b, y^b and z^b axes respectively.

According to Euler's law of rotation, the projection of the rotation angular velocity vector $\boldsymbol{\omega}_e^r$ in the rigid body coordinate system can be obtained as

$$\boldsymbol{\omega}_e^r = \begin{bmatrix}\omega_x^b \\ \omega_y^b \\ \omega_z^b\end{bmatrix} = \begin{bmatrix}-\dot{\psi}sin\varphi sin\theta - \dot{\theta}cos\varphi \\ -\dot{\psi}cos\varphi sin\theta + \dot{\theta}sin\varphi \\ \dot{\psi}cos\theta + \dot{\varphi}\end{bmatrix} \tag{22}$$

The moment of momentum of a rigid body can be expressed as

$$\boldsymbol{L}_{cr} = \boldsymbol{I} \cdot \boldsymbol{\omega}^b \tag{23}$$

Combining (20)-(23), the rotation equation when the rigid body rotates around the z^b-axis of the rigid body coordinate system is

$$I_z\dot{\omega}_z^b + (I_y - I_x)\omega_x^b\omega_y^b = M_{cz}^b \tag{24}$$

Among them: M_{cz}^b is the component of the principal torque M_c^b along the z^b-axis.

The expression of $\dot{\omega}_z^b$ can be obtained from (22). Since the research of guidance dynamics is mainly concerned with the lateral motion of the rigid body, so we substitute the expression of $\dot{\omega}_z^b$ into (24). The yaw motion equation of the rigid body relative to the track is further sorted out

$$I_z\ddot{\varphi} = M_{cz}^b + M_{ez}^b \tag{25}$$

Among them, $M_{ez}^{b} \approx -I_z V^2 \dot{\kappa} cos\theta$ is the traction torque of inertia of the rigid body, and the approximate equal sign is taken here because the formula is approximated by considering the track parameters to facilitate the next calculation. M_{cz}^{b} is the component of the principal torque of the rigid body on the z^b-axis.

To sum up the content of this section, the lateral motion equation of any single rigid body in the guidance system in the track coordinate system can be obtained from (26). The lateral motion equations of the guidance electromagnet, bogie and carriage can be calculated with reference to this formula. The difference between all kinds of rigid bodies is that the component F_{cy}^{r} of the resultant external force and the component M_{cz}^{b} of the principal torque are not same. Due to space limitations, this paper only gives general equations, and no longer derives specific lateral motion equations for each type of rigid body.

$$\begin{aligned} m\ddot{r}_y^r &= F_{cy}^r + F_{ey}^r \\ I_z\ddot{\varphi} &= M_{cz}^b + M_{ez}^b \end{aligned} \tag{26}$$

D. INTERACTION MODEL OF PRIMARY GUIDANCE SUSPENSION DEVICE

Considering that the primary suspension device located between the guidance electromagnet and the bogie allows the guidance electromagnet to deflect relative to the track. In order to describe the deflection, this section will analyze the effect of the guidance electromagnet suspension device and the bogie suspension device. Furthermore, the interaction model of primary guidance suspension device will be built.

It is worth noting that there is also a suspension device between the levitation electromagnet and the bogie. Due to the large damping of the device, the impact on the operation of the train's guidance system is very small, which can be ignored. Therefore, the suspension electromagnet and the bogie are regarded as a whole rigid.

A single primary guidance suspension device is taken as an example, as shown in Fig.12, to calculate the interaction of the device based on the deformation and stiffness of the device. Assuming that Fig.12 is the projection along the track surface when the rubber ball joints at both ends of the device. Points a_g and a_b are the characteristic points of the guidance electromagnet and the device on the bogie, namely the geometric center when the two ends of the ball joint are connected.

In order to facilitate analysis and calculation, a local coordinate system $o_1x_1y_1z_1$ of the device is established, where the origin o_1 is located at the midpoint of the line segment a_ga_b, and the x_1-axis and y_1-axis coincide with the horizontal and vertical axes of the rod, respectively. Since the radial rigidity of the device is large and the radial deformation is small, it can be approximately considered that the point o_1 coincides with the geometric center point of the rigid rod.

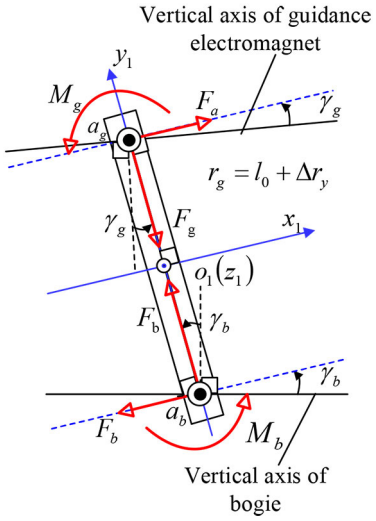

FIGURE 12. Interaction model of primary guidance suspension device.

The equivalent rigidity of the guidance primary suspension device can be obtained through equivalent calculation. The stiffness of the device along the y_1-axis, namely the radial stiffness is $C_y = 16.2kN/mm$. The universal torsional stiffness of the rubber ball joint at the end connected to the electromagnet and bogie are $C_{w1} = 20N \cdot m/deg$ and $C_{w2} = 53.4N \cdot m/deg$ respectively.

As shown in Fig.12, the radial deformation of the device along the y_1-axis is Δr_y, and the universal torsional deformations of the ball joints at both ends around the central axis of the ball joint parallel to the z_1-axis are γ_g and γ_b, respectively. The force of the bogie received from the device's radial deformation is F_b, and the torque of the universal torsional deformation from the device's ball joint is M_b. The guidance electromagnet receives the radial deformation force from the device as F_g, and the universal torsional torque from the device ball joint as M_g. In addition, when the rod of the device is in a state of torque balance, it will also be subjected to a torque of a moment. Two forces in the couple are provided by the axial stiffness and deformation of the ball joint along the axial direction of the ball joint at both ends. At this time, the guidance electromagnet and the bogie will also be respectively subjected to the component forces F_a, F_b,which leads the direction of the central axis of the ball joint parallel to the x_1-axis. The calculation formula for the above forces and torques is

$$\begin{aligned} F_g &= C_y \cdot \Delta r_y \\ F_b &= -F_g \\ M_g &= C_{w1} \cdot \gamma_g \\ M_b &= C_{w2} \cdot \gamma_b \end{aligned} \tag{27}$$

$$\begin{aligned} F_a &= (M_g + M_b)/(l_0 + \Delta r_y) \approx (M_g + M_b)/l_0 \\ &= -F_b \end{aligned} \tag{28}$$

Among them, l_0 is the original length of the device. Since $l_0 \gg \Delta r_y$, so $l_0 + \Delta r_y \approx l_0$

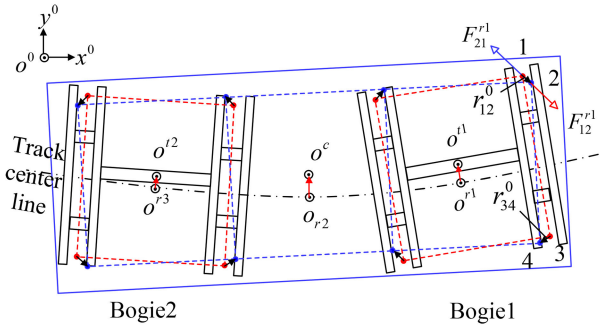

FIGURE 13. Interaction model of the secondary suspension device.

E. INTERACTION MODEL OF THE SECONDARY SUSPENSION DEVICE

1) DEVICE DEFORMATION CALCULATION

According to the analysis in section II, the lateral equivalent stiffness of the secondary suspension device is formed by the parallel equivalent stiffness of the pendulum rod and the stiffness of the y-direction spring. Suppose that the lateral equivalent stiffness is known, the effect of the device on the adjacent rigid body depends on the projection along the rail surface when the pendulum rod swings. In order to simplify the study, when calculating the movement of the pendulum, suppose that the cross slope angle of the line is zero, and each rigid body is projected to the $x_0 - y_0$ plane of the inertial coordinate system. As shown in Fig.13, the outermost rectangular frame represents the projection of the carriage on the $x_0 - y_0$ plane, and the two inner rigid structures represent the projection of the two bogies on the $x_0 - y_0$ plane.

In the following content, the secondary suspension device of the bogie 1 and bogie 2 will be taken as an example. The calculation method of the deformation of the secondary suspension device is given.

First of all, the track coordinate system and the rigid body coordinate system are established. As shown in Fig. 13, o^{r1},o^{r2},o^{r3}represent the three track coordinate systems. o^{t1}, o^{t2} represent the rigid body coordinate system of the two bogies. o^c represents the rigid body coordinate system of the carriage. Points 1 and 3 represent the equivalent points of the installation position of the secondary suspension device on the bogie 1. Points 2 and 4 represent the equivalent points of the installation position of the secondary suspension device on the carriage.

In the bogie rigid body coordinate system o^{t1}, the position vectors of point 1 and point 3 are

$$\begin{aligned} \mathbf{r}_1 &= \begin{pmatrix} l_{pt} & w_{pt} & 0 \end{pmatrix} \\ \mathbf{r}_3 &= \begin{pmatrix} l_{pt} & -w_{pt} & 0 \end{pmatrix} \end{aligned} \tag{29}$$

where, l_pt and w_{pt} are parameters of bogie 1.

In the carriage rigid body coordinate system o^c, the coordinate position vector of the 2 and 4 points is

$$\begin{aligned} \mathbf{r}_2 &= \begin{pmatrix} 3l_{pt} & w_{pt} & 0 \end{pmatrix} \\ \mathbf{r}_4 &= \begin{pmatrix} 3l_{pt} & -w_{pt} & 0 \end{pmatrix} \end{aligned} \tag{30}$$

According to the coordinate transformation relationship, the position vector of points 1, 2, 3, 4 in the inertial coordinate system can be obtained

$$\begin{aligned} \mathbf{r}_1^0 &= \mathbf{r}_{r1}^0 + \mathbf{A}_{r1}^0 \mathbf{r}_{t1}^r + \mathbf{A}_{t1}^0 \mathbf{r}_1 \\ \mathbf{r}_2^0 &= \mathbf{r}_{r2}^0 + \mathbf{A}_{r2}^0 \mathbf{r}_c^r + \mathbf{A}_c^0 \mathbf{r}_2 \\ \mathbf{r}_3^0 &= \mathbf{r}_{r1}^0 + \mathbf{A}_{r1}^0 \mathbf{r}_{t1}^r + \mathbf{A}_{t1}^0 \mathbf{r}_3 \\ \mathbf{r}_4^0 &= \mathbf{r}_{r2}^0 + \mathbf{A}_{r2}^0 \mathbf{r}_c^r + \mathbf{A}_c^0 \mathbf{r}_4 \end{aligned} \tag{31}$$

thus, the deformation vector that can represent the secondary suspension device is obtained

$$\begin{aligned} \mathbf{r}_{12}^0 &= \mathbf{r}_2^0 - \mathbf{r}_1^0 \\ \mathbf{r}_{34}^0 &= \mathbf{r}_4^0 - \mathbf{r}_3^0 \end{aligned} \tag{32}$$

2) DEVICE INTERACTION CALCULATION

Taking the first secondary suspension device of the right suspension frame as an example, the vector of the force of the device on the bogie in the track coordinate system o^{r1} is F_{12}^{r1}, and the vector of the force on the carriage in the track coordinate system o^{r1} is F_{21}^{r1}. The lateral stiffness of the secondary suspension device is synthesized by the equivalent stiffness of the pendulum rod and the stiffness of the y-direction spring. Suppose that the vertical load borne by the device is F_p, the equivalent stiffness C_b of the device along the r_{12} direction can be obtained as

$$C_b = C_p + C_{Ys} = \frac{F_p}{\sqrt{L_p^2 - |\mathbf{r}_{12}^0|^2}} + C_{Ys} \tag{33}$$

where C_{Ys} is the equivalent stiffness of the y-direction spring. L_p is the center distance of the ball joint at both ends of the pendulum rod, $|\mathbf{r}_{12}^0| = \sqrt{(r_{12x}^0)^2 + (r_{12y}^0)^2}$. r_{12x}^0 and r_{12y}^0 are the projections of r_{12} along the x^0-axis and y^0-axis of the inertial coordinate system, respectively.

Therefore, the force of the device on the bogie can be obtained as

$$\mathbf{F}_{12}^{r1} = C_b \mathbf{A}_0^{r1} \mathbf{r}_{12}^0 \tag{34}$$

Among them, $\mathbf{A}_0^{r1}$ is the rotation transformation matrix from the inertial coordinate system to the track coordinate system.

IV. CONTROL STRATEGY OF GUIDANCE SYSTEM

In order to ensure the lateral stability of the guidance system and the safety of curve passing while the maglev is running at high speed, the strategy of active guidance control is adopted. The guidance system of the train consists of guidance electromagnets arranged on both sides of the maglev, as shown in Fig.14. Each guidance electromagnet is connected to the bogie through two sets of guidance primary suspension devices. Therefore, the relative motion between the electromagnet and bogie is allowed. This modular mechanical decoupling structure makes the decentralized control of the guidance system possible. The control problem of the maglev guidance system can be decomposed into the control problem of a single guidance electromagnet on both sides of the maglev.

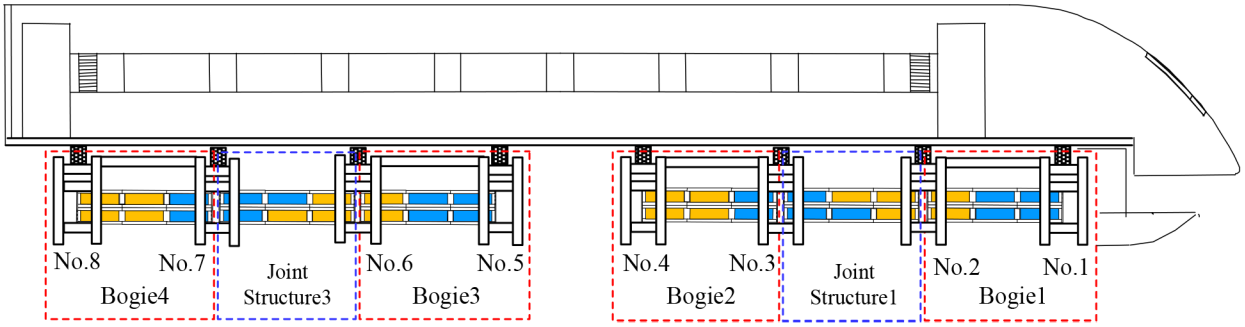

FIGURE 14. Grouping assignment of guidance control units in a maglev train

A. CONSIST OF GUIDANCE CONTROL SYSTEM

Fig.14 shows the grouping of the magnetic poles of the guidance electromagnets of whole maglev. The guidance magnetic pole coils of the same color are connected in series, corresponding to a guidance control unit. Each guidance control unit is composed of sensors, controllers, choppers and electromagnets. There are two different type of sensors including the gap sensor and the current transformers. The gap sensor is installed on the electromagnet to measure the gap signal δ and acceleration signal of the electromagnet a. The current transformer is installed in the chopper to measure the current signal i of the electromagnet coil. The function of the controller is mainly to generate a PWM control signal to drive the chopper according to the control algorithm. The chopper can amplify the PWM control signal into the drive voltage of the coil.

The basic goal of guidance control is to ensure the stability of the maglev's lateral gap and make the maglev run through the center of line of track. At present, the following control strategy is commonly used: independent control is adopted in two sets of magnetic poles located in the same electromagnet; Bilateral differential control is adopted in two sets of magnetic poles located in the different electromagnet located in left and right side of train.

Three guidance control units contained in the floating frames No. 7 and No. 8 are taken as an example, the basic control strategy is shown in Fig.15. The work Features of this system mainly includes: the guidance control units on the different suspension frames No. 7 and No. 8 are completely independent in control, and there is no information interaction; The guidance units located on the same suspension frame, namely the No. 7 suspension frame, exchange gap signals through the RS485 communication interface under the vehicle. The redundancy of the gap signal is improved, moreover, the system reliability is also enhanced.

In addition, the control units symmetrically distributed on both sides of the track also exchange gap information through the RS485 communication interface.The control target is to make the difference of the gap signals on left and right side become zero.

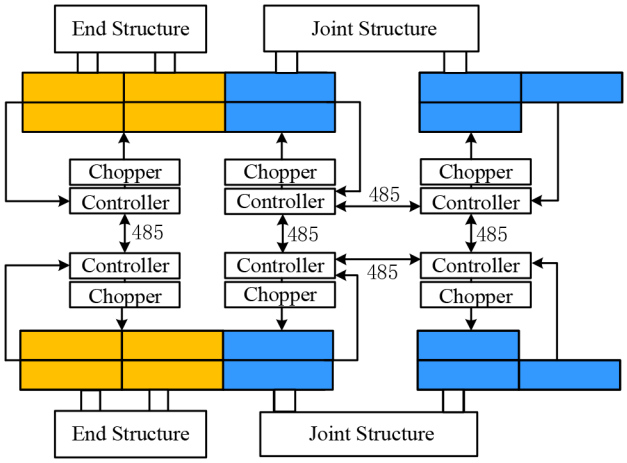

FIGURE 15. Control strategy and signal flow in Bogie 4.

B. EQUIVALENT OF GUIDANCE CONTROL UNIT AND DESIGN OF CONTROL ALGORITHM

In practical engineering applications, the guidance control unit realizes the control of the input voltage u of coil based on the guidance gap δ from gap sensor, acceleration a, and coil current i. Physical links such as wave devices. Considering that the physical realization of these links is complicated, it may as well be abstracted into modular functions when conducting theoretical research and simulation analysis. The equivalent of a control unit is shown in Fig.16, where: the physical quantities represented by each symbol are regarded as continuous quantities. u is the input voltage of coil. $\hat{u}$ is the expected voltage obtained by the control algorithm according to the state feedback quantity of the controller; k_u is the forward gain of the control quantity output of PWM; k_r is the equivalent gain of the chopper.

In order to ensure that the actual value u of the voltage is consistent with the expected value $\hat{u}$, it should satisfy: $k_u k_r = 1$. At this time, the model of the guidance control unit mainly depends on the control algorithm and the saturation link of the chopper, where the output of the saturation link of the chopper satisfies: $u < 440V$.

Voltage is taken as the control object in the guidance control. Gap signal, acceleration signal and current signal

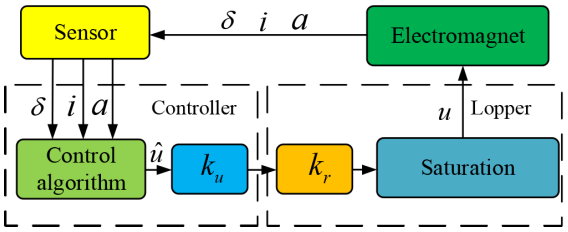

FIGURE 16. Equivalent of a guidance control unit.

are adopted as variable of feedback states. in order to eliminate the gap error, the integration link is also introduced. In order to facilitate the realization of control algorithms, linear controllers are mostly used in practical applications at present. A common algorithm for controllers under the control strategy shown in Fig.16 is

$$\begin{cases} u_l = u_0 + k_p \dfrac{\delta_l - \delta_r}{2} + k_i \int_0^t (\dfrac{\delta_l - \delta_r}{2}) dt + k_v \dot{\delta}_l + k_c (i_l - i_0) \\ u_r = u_0 + k_p \dfrac{\delta_r - \delta_l}{2} + k_i \int_0^t (\dfrac{\delta_r - \delta_l}{2}) dt + k_v \dot{\delta}_r + k_c (i_r - i_0) \end{cases} \tag{35}$$

Among them: i_0 is the static current of the controller, $u_0 = i_0 R$ is the static voltage, R is the equivalent resistance of the magnetic coil. k_p, k_i and k_v are the ratio, integral and speed feedback coefficients of gap respectively. k_c is current feedback coefficient.

V. SIMULATION AND RESULTS

A. SIMULATION MODEL STRUCTURE

In this section, the guidance system of high-speed maglev train will be modeled and simulated. The simulation model structure is shown in Fig.17. The simplified maglev train system includes a total of 17 rigid bodies, and there are 34 degrees of freedom of motion in the study of guidance dynamics. Therefore, there are 34 equations in this model. Because of the limitation of space, only the class name of equation and their relationship are shown in Fig.17.

The running logic of the simulation model can be divided into the following 6 steps:

1) The line model is used as the driving data for the simulation model of the guidance system.
2) The track parameter acts on the lateral motion equation of the guidance electromagnet, which makes the guidance electromagnet deviation and yaw relative to the track. In the meanwhile, the voltage of electromagnet will be changed in the guidance control unit, correspondingly, the electromagnetic force in the electromagnet motion equation will be changed.
3) The deviation of the guidance electromagnet makes the connected guidance primary suspension device find deformation and produce deformation force.
4) The deformation force of the guidance primary suspension device acts on the bogie, making the bogie deviate and yaw relatively to the track.

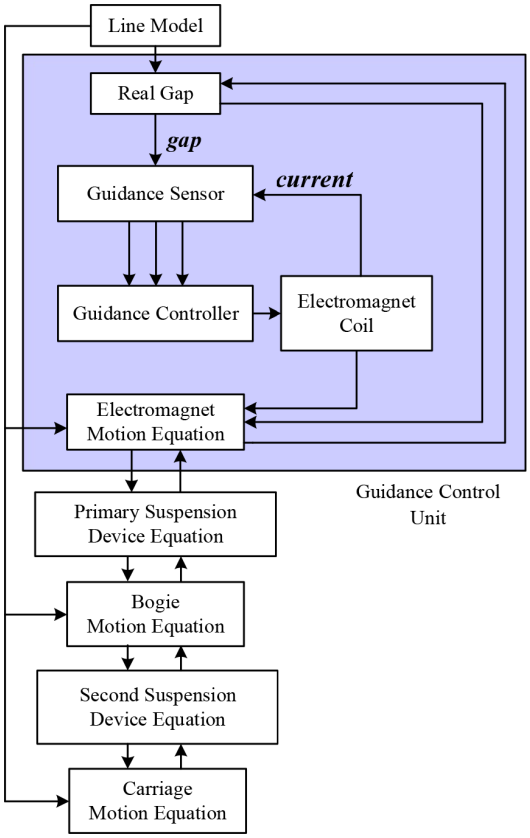

FIGURE 17. Block diagram of simulation model.

5) The deflection of the bogie will cause deformation of the secondary suspension device connected to it, resulting in deformation force.
6) Four bogies in a maglev act together on the carriage through the secondary suspension device, which makes the carriage laterally deviation and yaw relative to the track.

The process of the high-speed maglev train passing through a curve can be simulated by importing the parameters of line model. The guidance dynamics characteristics of rigid bodies and the working state of each guidance unit can be obtained through this simulation.

Assuming that the total weight of the carriage is m_c which is evenly distributed along the floor of the carriage. The height and pressure of each air spring are equal and always remain unchanged. Since the effective bearing area of the air spring at the end of the train is half of the middle one, the vertical load of the pendulum rod at positions No.1 and No.8 in Fig.14 will be $m_c g/28$. The vertical load at other positions is $m_c g/14$. It is known that the y-direction spring in the secondary suspension device at the suspension frame unit No. 1, 4, 5 and 8 is a limit spring, which only works when the displacement exceeds 90 mm.

B. SIMULATION RESULTS ANALYSIS

Suppose the operation speed is 25 km/h.Put the line model shown in Fig.8 into guidance system dynamics model.

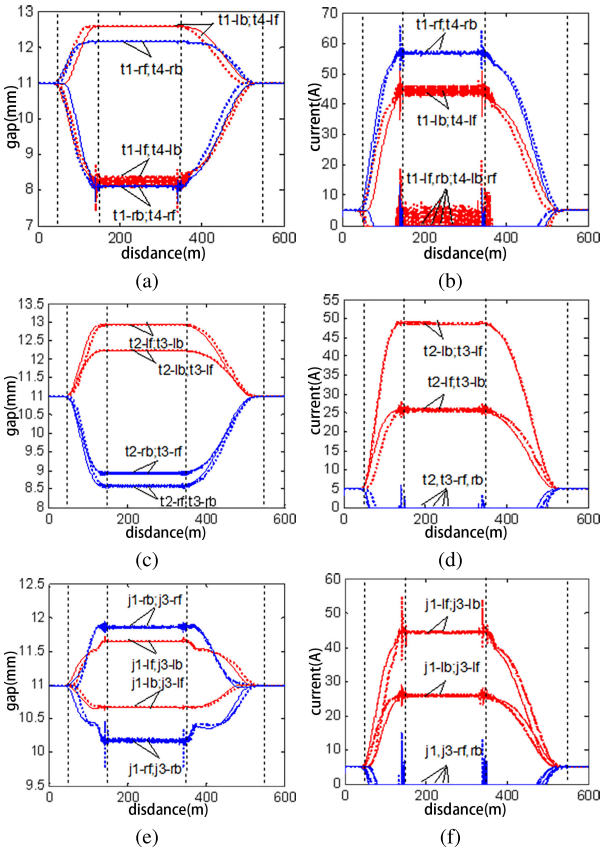

FIGURE 18. Guidance gap and current of the control units in simulation. (a) Guidance gap of bogie 1(t1) and bogie 4(t4). (b) Guidance current of bogie 1(t1) and bogie 4(t4). (c) Guidance gap of bogie 2(t2) and bogie 3(t3). (d) Guidance current of bogie 2(t2) and bogie 3(t3). (e) Guidance gap of joint structure1(j1) and joint structure3(j3). (f) Guidance current of joint structure1(j1) and joint structure3(j3).

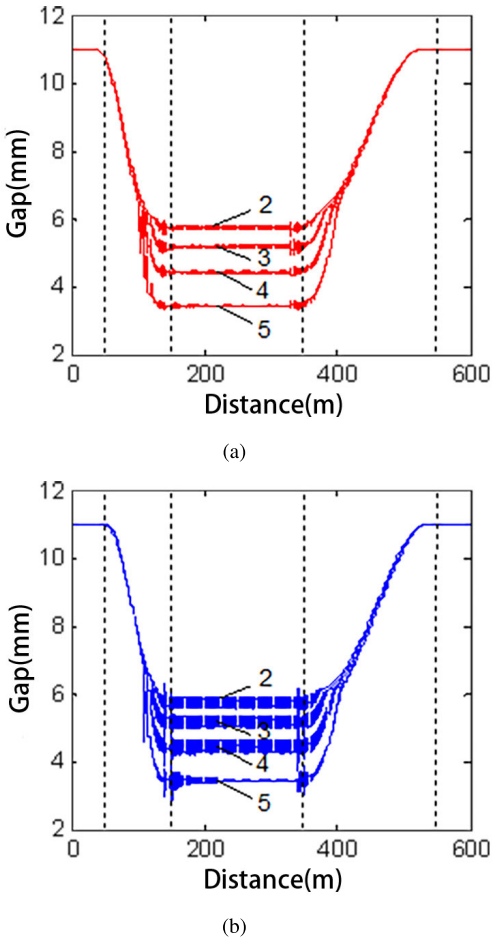

FIGURE 19. Guidance gap of guidance control units on the left side of the maglev at the speed of 25 km/h, 50 km/h, 75 km/h and 100 km/h, corresponding to the curve masked 2, 3, 4 and 5. (a) Front-end of maglev (b) Back-end of maglev.

We can get the working state of the guidance control unit, namely guidance gap and current from the simulation results, as shown in Fig.18. Among the symbols in each type of curve, the prefix $t_m(m = 1, 2, 3, 4)$ represents the bogie numbered $1, 2, 3, 4$; $j_n(n = 1, 3)$ represents the guidance joint structure numbered 1 and 3. The suffixes lf, lb, rf, rb represent the left front end, left back end, right front end and right back end respectively. The solid and dashed lines are used to distinguish the guidance control unit at the front and back of the bogie or joint structure. Red and blue color are used to distinguish the guidance control unit on the left and right side of the maglev.

It can be seen from Fig.18 that at speed of 25 km/h, the guidance control unit, distributes along the horizontal axis of the middle of the car symmetrically, corresponds to the similar gap and current change rules in whole line without in the transition curve, moreover the difference in the transition curve is very small. For instance, the curve of t1-lb and t4-lf in Fig.18(a) are coincide almostly. The gap and current of the right front end (t1-rf) and left back end (t1-lb) of the bogie No.1 in the curve, the right back end (t4-rb) and the left front end (t4-lf) of the bogie No.4 have increased, and the increase in the current on the right is always greater than that on the left. When the train enters the circular curve from the transition curve, under the action of the y-direction limit spring in the secondary suspension device, the gap at each control unit will fluctuate lightly.

According to the above simulation results, it can be seen that the edge points of the guidance electromagnets at both ends of the system near the left side of the curve, namely the position t1-lf and t4-lb, will be the closest to the track when the maglev guidance system passes through the curve section.

Change the operation speed from 25 km/h to 100km/h. The guidance gap curves of the position t1-lf and t4-lb is shown in Fig.19.

It can be seen from the result that as the speed increases, the reduction of guidance gap at the inner end edge of the curve will increase. Therefore, the front and back end of bogie are more likely to collide with the track, which is consistent with the position in the actual train.

Through the above simulation and analysis, the working state of the guidance system of the maglev train is obtained. The guidance gaps of the front and back end bogie of the train at different speeds are simulated. Further the cause of the

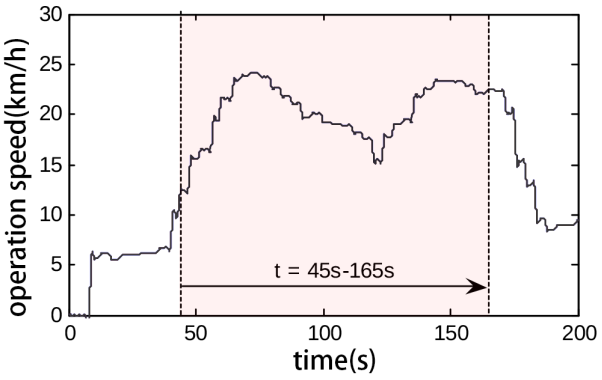

FIGURE 20. Test curve of the system traction speed. Curve between t = 45s and t = 165s corresponds to the line in the simulation.

collision between the guidance electromagnet and the track during the actual train operation is analyzed.

VI. ACTUAL RUNNING TEST

A. TEST CONDITION

The high-speed maglev experimental vehicle was manufactured by CCRC Changchun Railway Vehicles Corporation. The design indicators such as the dimensions and system functions of the experimental prototype are basically the same as those of the German TR08-type maglev train.

The operation test of the maglev train system was completed on the 1.5 km long line of the Shanghai Jiading High-speed maglev Test Base. All guidance controllers are connected via the vehicle's CAN bus. By using the upper computer connected to the USB-CAN acquisition box, the guidance control state data sent by the controller is obtained and stored. Although the data transmission rate of the debugging bus is limited and the update interval of the test data is large, the drawn curve is sufficient to reflect the basic change of the guidance state when the train is turning, especially the change law of the current. The following step is to paint the test curves according to the test datas.

B. TEST CURVE AND ANALYSIS

In the operation test, the experimental vehicle entered the traction operation state from the static guidance state from the straight section, and passed the first curve of the line. The test curve of the system traction speed change is shown in Fig.20. In order to make a contrast of the test data and the simulation, the t = 45-165 s running time period is intercepted, which contains the running process of the train entering and leaving the first curve. The maximum operation speed of the curve passing is close to 25 km/h.

Through the test, the corresponding guidance working state data of each bogie system and joint structure are collected. Due to the limitation of space in this paper, the representative guidance units are selected and the test curves of guidance gap and guidance current are drawn, as shown in Fig.21-Fig.24.

When a single train passes the curve, as shown in Fig.21(b)(d), the guidance current at left front and back

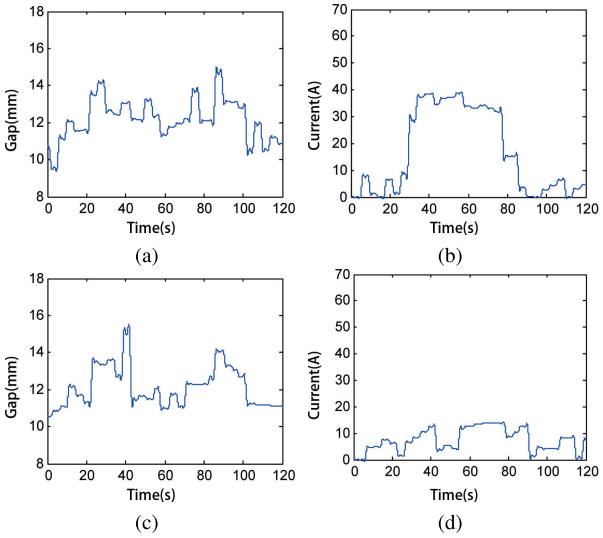

FIGURE 21. Guidance gap and current of control units in joint structure 1. (a) Gap of left-front-end control unit. (b) Current of left-front-end control unit. (c) Gap of left-back-end control unit. (d) Current of left-back-end control unit.

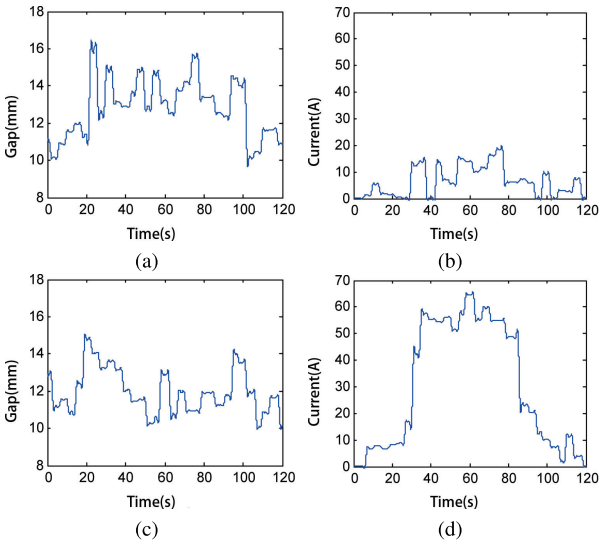

FIGURE 22. Guidance gap and current of control units in bogie 2. (a) Gap of left-front-end control unit. (b) Current of left-front-end control unit. (c) Gap of left-back-end control unit. (d) Current of left-back-end control unit.

ends of joint structure 1 and 3 has increased, among which, the increase of guidance current adjacent to bogie system 1 and 4 is larger. In addition, as shown in Fig.24(a) and Fig.23(a), it can be seen that the gap between the guide control units at both ends of the system close to the left side of the curve is significantly reduced, and the reduction of the clearance of the control unit at the back of the train is greater.

As shown in Fig.22(b)(d), the guidance current at the front and back ends of the left side of the bogie system 2 and 3 increases, among which the guidance current near the eddy current braking position in the middle of the train increased largely.

The gap and current of the guidance control unit at the right front end and left back end of the bogie system 1 and

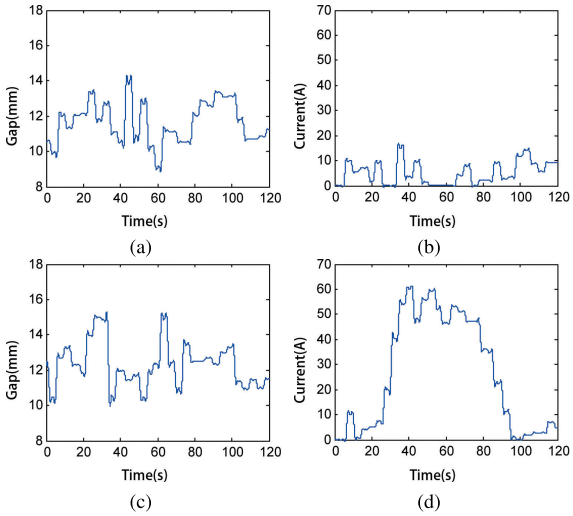

FIGURE 23. Guidance gap and current of control units in bogie 1. (a) Gap of left-front-end control unit. (b) Current of left-front-end control unit. (c) Gap of right-front-end control unit. (d) Current of right-front-end control unit.

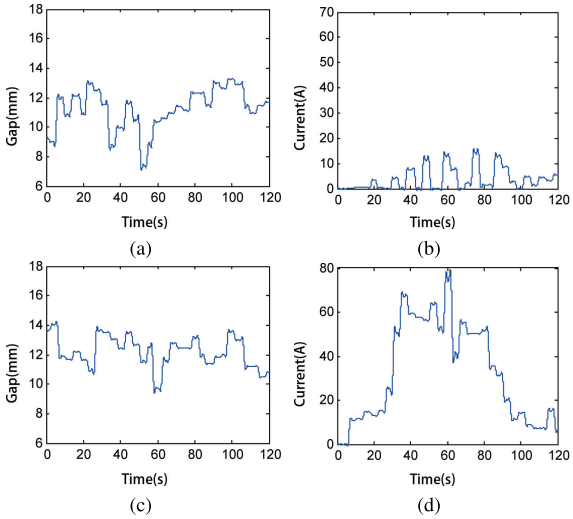

FIGURE 24. Guidance gap and current of control units in bogie 4. (a) Gap of left-back-end control unit. (b) Current of left-back-end control unit. (c) Gap of right-back-end control unit. (d) Current of right-back-end control unit.

the right back end and left front end of the bogie system 4 are significantly increased as shown in Fig.23(b)(d) and Fig.24(b)(d).

Due to the difference between the operating conditions of the train and the ideal situation set in the simulation, there is a deviation between the test results and simulation results, especially in the amplitude of the guidance working state. To clarify more specifically, there are three aspects: 1) The deviation of guidance gap is mainly caused by the large mechanical installation error between the actual guidance electromagnet and the gap sensor; 2) When the actual train is running, the increase of guidance current at the tail of the train outside the curve is slightly larger than the head of the train. It is caused by the uneven vertical load distribution at the head and tail of the actual train; 3) Compared with the simulation results, the current in the end adjacent to the eddy current braking position increases larger than the other end. The main reason is that the eddy current brake electromagnet will generate force and torque on the adjacent bogie through the connecting device when the train is turning.

In addition, according to the simulation conclusion in Fig.18, when the train is turning, the gap between the ends of the guidance electromagnets, at both ends of the vehicle system close to the inner side of the curve, has the largest reduction. This position may collide with the track first, which is corresponding to the actual running test.

Combining the above analysis, it can be concluded that the effectiveness of the simulation results and the rationality and usability of the guidance dynamics model are verified by the test results.

VII. CONCLUSION

In this paper, first of all, we analyzed the structure of the high-speed maglev train guidance system, and established a parametric mathematical model for the main components. Then, according to the multi-rigid body dynamics theory, the dynamics modeling of the high-speed maglev train guidance system was carried out: The lateral motion equation of the rigid body was obtained; the interaction law of the guidance primary suspension device and the secondary suspension device was obtained. Thirdly, a dynamics simulation model of the whole guidance system was established; The process of the high-speed maglev train passing through a curve was simulated to obtain the working state of the guidance system. The guidance gaps of the front and back bogies of the train at different speeds are analyzed, and the cause of the friction between the guidance electromagnet and the track during the actual train operation is found.

Finally, vehicle operation test is conducted on the high-speed maglev experiment line in Jiading, Shanghai. Test data were collected and analyzed, which preliminarily verified the rationality and usability of the guidance dynamics model established in this paper. The experimental data show that the dynamics model of the guidance system of the high-speed maglev train established in this paper can reflect the real guidance working state and give a reliable explanation of the problem happened in the actual test.

At present, China is developing a new generation of high-speed maglev train with a speed of 600 km/h. The dynamics model of the guidance system established in this paper can provide a reliable platform for the research of the guidance control algorithm and the analysis of the dynamics characteristics of the maglev, further more promote the application of the new generation maglev.

REFERENCES

[1] G. Lin and X. Sheng, "Application and further development of maglev transportation in China," *Transp. Syst. Technol.*, vol. 4, no. 3, pp. 36–43, Nov. 2018.

[2] M. Janic, "Multicriteria evaluation of high-speed rail, transrapid maglev and air passenger transport in europe," *Transp. Planning Technol.*, vol. 26, no. 6, pp. 491–512, Dec. 2003.

[3] H.-W. Lee, K.-C. Kim, and J. Lee, "Review of maglev train technologies," *IEEE Trans. Magn.*, vol. 42, no. 7, pp. 1917–1925, Jul. 2006.

[4] Y. Luguang, "Progress of the maglev transportation in China," *IEEE Trans. Appl. Supercond.*, vol. 16, no. 2, pp. 1138–1141, Jun. 2006.

[5] L. Yan, "Development and application of the maglev transportation system," *IEEE Trans. Appl. Supercond.*, vol. 18, no. 2, pp. 92–99, Jun. 2008.

[6] A. Hao, Z. Long, and W. Chang, "Design of the robust controller of the guidance system in high-speed maglev train," *J. China Railway Soc.*, vol. 30, no. 6, pp. 40–45, 2008.

[7] A. Hao, L. She, and W. Chang, "Adaptive controller design of guidance system of EMS high speed maglev train," *Control Eng. China*, vol. 15, no. 2, pp. 116–119, 2008.

[8] M. Zhai, A. Hao, X. Li, and Z. Long, "Research on the active guidance control system in high speed maglev train," *IEEE Access*, vol. 7, pp. 741–752, 2019.

[9] B. Li, X. Li, and Z. Long, "Design of model reference adaptive controller for active guidance system of high speed maglev train," in *Proc. Chin. Control Decis. Conf. (CCDC)*, Aug. 2020, pp. 945–950.

[10] C.-H. Kim, C.-W. Ha, J. Lim, H.-S. Han, and K.-J. Kim, "Yaw motion control of electromagnetic guidance system for high-speed maglev vehicles," *J. Electr. Eng. Technol.*, vol. 11, no. 5, pp. 1299–1304, Sep. 2016.

[11] M. Kim, J.-H. Jeong, J. Lim, C.-H. Kim, and M. Won, "Design and control of levitation and guidance systems for a semi-high-speed maglev train," *J. Electr. Eng. Technol.*, vol. 12, no. 1, pp. 117–125, Jan. 2017.

[12] J.-D. Lee, Z.-B. Wang, J.-Q. Lu, X.-R. Chen, and R.-Y. Duan, "Cascade control strategy design for electromagnetic guidance system," in *Proc. 6th IEEE Conf. Ind. Electron. Appl.*, Jun. 2011, pp. 2803–2808.

[13] C. Zhao, L. She, and W. Chang, "Research on guidance system for single bogie of high-speed maglev train in the curve negotiation," *J. China Railway Soc.*, vol. 33, no. 7, pp. 32–37, 2011.

[14] Y. Wu, "Guidance control system and simulation research of EMS type high-speed maglev vehicle," *J. Heilongjiang Inst. Sci. Technol.*, vol. 16, no. 4, pp. 244–247, 2006.

[15] X. Ye, "Modeling and simulation analysis of maglev vehicle system dynamics," Ph.D. dissertation, Nat. Key Lab. Traction Power, Southwest Jiaotong Univ., Chengdu, China, Mar. 2007.

[16] B. Miao, S. Xiao, S. Luo, D. Jin, and C. Lei, "Modeling and simulation of maglev vehicle structure dynamics," *China Railway Sci.*, vol. 27, no. 1, pp. 104–108, 2006.

[17] Y. Deng, S. Luo, H. Liang, and W. Ma, "Simulation model of maglev coupling dynamics performance based on SIMPACK," *J. Traffic Transp. Eng.*, vol. 7, no. 1, pp. 12–15 and 20, 2007.

[18] M. Piao, S. Liang, S. Xue, and W. Zhao, "2-DOF control of active levitation and guidance in high-speed maglev train," *China Railway Sci.*, vol. 27, no. 4, pp. 80–85, 2006.

[19] M. Piao, Y. Cao, S. Liang, and W. Zhao, "Assembled model and guidance principle of high-speed maglev train," *China Railway Sci.*, vol. 29, no. 4, pp. 103–108, 2008.

[20] J. Wang, M. Piao, and W. Zhao, "Curve-matching dynamic performance of high-speed maglev trainset," *Railway Locomotive Car*, vol. 27, no. 1, pp. 82–86, 2007.

[21] T. Ma, "The study on stability of levitation and guidance active control in high-speed maglev train," Ph.D. dissertation, College Locomotive Vehicle Eng., Dalian Jiaotong Univ., Dalian, China, 2005.

[22] H. Wu, "Study on performance of high-speed maglev vehicle running on small radius curve," Ph.D. dissertation, College Locomotive Vehicle Eng., Dalian Jiaotong Univ., Dalian, China, 2007.

BOWEN LI received the B.Eng. degree from the College of Mechanical and Vehicle Engineering, Hunan University, Changsha, in 2018. He is currently pursuing the M.S. degree in control science and engineering with the National University of Defense Technology, Changsha, China. His current research interests include magnetic levitation control, guidance system control, and the dynamics of the guidance system of maglev.

CHUNXIA ZHAO received the B.S. degree in automation from Northeastern University, Liaoning, China, in 2004, the M.S. degree in control science and engineering from the National University of Defense Technology, Changsha, China, in 2006, and the Ph.D. degree in control science and engineering from the National University of Defense Technology, Changsha, in 2014. Her research interests include magnetic levitation control and dynamics of guidance system of maglev.

XIAOLONG LI received the Ph.D. degree in control science and engineering from the National University of Defense Technology, Changsha, China, in 2009. He works with the National University of Defense Technology as an Associate Research Fellow. His research interests include magnetic levitation control and new maglev technology.

ZHIQIANG LONG received the B.S. degree in automation from the Huazhong University of Science and Technology, Wuhan, China, in 1988, the M.S. degree in flight mechanics from the Harbin Institute of Technology, Harbin, China, in 1991, and the Ph.D. degree in control science and engineering from the National University of Defense Technology, Changsha, China, in 2010.

He is currently a Professor with the National University of Defense Technology, where he is also the Head Research Engineer with the Engineering Research Center of Maglev Technology. His research interests include magnetic levitation control, fault diagnosis, and new maglev technology.